Research Article

Chemical Review and Letters
journal homepage: www.chemrevlett.com
ISSN (online): 2645-4947 (print) 2676-7279

DFT studies on the nalidixic acid interactions with $C_8B_6N_6$ nanocluster

Ali Behnia[1], Mohammad Reza Jalali Sarvestani[2,*], Azher abdulmutaleb ibrahim[3], Morug Salih Mahdi[4]

[1]*Faculty of Pharmacy, University of Szeged, Eötvös u 6., 6720 Szeged, Hungary*
[2]*Young Researchers and Elite Club, Yadegar-e-Imam Khomeini (RAH) Shahr-e-Rey Branch, Islamic Azad University, Tehran, Iran*
[3]*Al-Zahrawi University College, Karbala, Iraq*
[4]*College of MLT Ahl Al Bayt University Iraq*

ARTICLE INFO

Article history:
Received 11 September 2024
Received in revised form 4 October 2024
Accepted 8 October 2024
Available online 4 December 2024

Keywords:
Nalidixic acid
$C_8B_6N_6$ fullerene
DFT
Adsorption

ABSTRACT

The study examined the effectiveness of $C_8B_6N_6$ nanoclusters in acting as both an adsorbent and sensor for removing and detecting nalidixic acid (NA) using density functional theory computations. The findings indicated that the interaction between NA and $C_8B_6N_6$ is feasible, exothermic, and spontaneous, highlighting the potential of $C_8B_6N_6$ as an efficient adsorbent for NA removal. The research also investigated the impact of water as the solvent and varying temperature on the thermodynamic parameters, revealing no significant influence on the interactions. Additionally, the Frontier Molecular Orbital (FMO) analysis revealed notable changes in the bandgap of $C_8B_6N_6$ from 8.09 (eV) to 5.46 (eV) (-32.46%) during the adsorption process, suggesting its potential use as an effective electrocatalytic modifier for the electrochemical detection of NA. Other FMO parameters were also discussed in details. Overall, this study provides valuable insights into the potential use of $C_8B_6N_6$ as an efficient adsorbent and sensor for the removal and detection of NA.

1. Introduction

Nalidixic acid (NA, Fig. 1) is an important compound that requires careful determination and removal due to its potential impact on human health and the environment [1]. As a synthetic antibiotic, NA has been widely used to treat urinary tract infections caused by susceptible bacteria [2]. However, its overuse and improper disposal can lead to environmental contamination and the development of antibiotic-resistant strains of bacteria [3]. The determination of NA in various matrices, such as water, soil, and biological samples, is crucial for assessing its presence and potential risks [4]. Analytical methods including high-performance liquid chromatography (HPLC) and mass spectrometry are commonly employed to accurately quantify NA levels [5]. These methods enable researchers and regulatory agencies to monitor its occurrence and establish guidelines for acceptable concentrations in different environmental compartments [6].

Once NA is detected, appropriate removal strategies must be implemented to mitigate its adverse effects [7]. Advanced oxidation processes, such as ozonation and photocatalysis, have shown promise in degrading NA in water treatment facilities [8]. Additionally, bioremediation techniques utilizing microorganisms capable of metabolizing NA have been explored for soil and sediment remediation [9]. Furthermore, the proper disposal of pharmaceutical formulations containing NA is essential to prevent its release into the environment [10]. Pharmaceutical manufacturers and healthcare facilities should adhere to regulations governing the handling and disposal of expired or unused medications to minimize the potential impact of NA on ecosystems and human health. Electrochemical sensors offer several advantages over high-performance liquid chromatography (HPLC) and mass spectrometry [11]. Firstly, electrochemical sensors are known for their high sensitivity, allowing for the detection of analytes at very low concentrations [12]. The adsorption technique has been extensively studied as an efficient method for various applications, including drug

* Corresponding author; e-mail: Rezajalali93@yahoo.com
https://doi.org/10.22034/crl.2024.478064.1418

delivery, where it facilitates drug absorption; environmental remediation, where it aids in removing pollutants to protect the environment; and industrial processes, such as gas storage, separation, and catalysis [13]. Additionally, adsorption can be easily tailored to target specific antibiotics by using different types of adsorbent materials, allowing for a more targeted and efficient removal process [14]. Furthermore, adsorption is a cost-effective method compared to other techniques such as advanced oxidation or membrane filtration [15]. The relatively low cost of adsorbent materials and the simplicity of the adsorption process make it an attractive option for large-scale antibiotic removal applications. In addition, adsorption can be easily integrated into existing water treatment systems, minimizing the need for major infrastructure changes or upgrades [15]. Another advantage of adsorption is its ability to remove antibiotics without producing harmful by-products or secondary pollutants [16]. Unlike some chemical treatment methods, adsorption does not involve the use of harsh chemicals or the generation of toxic residues, making it a more environmentally friendly option for antibiotic removal [17]. Moreover, adsorption processes are generally robust and tolerant to variations in water quality and operating conditions. This means that adsorption can effectively remove antibiotics from water and wastewater even in the presence of other contaminants or fluctuating pH and temperature levels, providing a reliable and consistent treatment performance [18]. $C_8B_6N_6$ nanocluster (Fig. 1), also known as boron carbon nitride, possesses unique properties that make it an exceptional sensor and adsorbent [18]. This nanocluster has a high surface area and a large number of active sites, allowing it to effectively adsorb various molecules and ions [19]. Its high reactivity and selectivity make it an ideal candidate for sensing applications, as it can detect specific analytes with high sensitivity. Additionally, $C_8B_6N_6$ nanocluster exhibits excellent stability and robustness, making it suitable for long-term sensing and adsorption processes [20]. The electronic structure of $C_8B_6N_6$ nanocluster also contributes to its exceptional performance as a sensor and adsorbent. Its unique combination of boron, carbon, and nitrogen atoms results in a well-defined electronic band structure, which enables efficient charge transfer and interaction with target molecules [21]. This property enhances its ability to selectively bind to specific analytes, making it a valuable tool for detecting and removing contaminants from various environments [22]. Furthermore, the tunable nature of $C_8B_6N_6$ nanocluster allows for customization of its properties to suit specific sensing and adsorption requirements [23]. By adjusting the composition and structure of the nanocluster, its affinity towards certain molecules can be enhanced, leading to improved sensing and adsorption capabilities [24]. This versatility makes $C_8B_6N_6$ nanocluster a versatile platform for a wide range of applications, including environmental monitoring, biomedical diagnostics, and industrial purification processes. In addition to its exceptional sensing and adsorption capabilities, $C_8B_6N_6$ nanocluster also exhibits remarkable chemical and thermal stability [25]. This property ensures that the nanocluster can withstand harsh environmental conditions and prolonged exposure to high temperatures, making it suitable for demanding sensing and adsorption applications. Its robust nature allows for continuous operation without degradation, providing reliable and consistent performance over extended periods [26]. Moreover, the scalable synthesis of $C_8B_6N_6$ nanocluster makes it readily accessible for large-scale production, further enhancing its potential for widespread use as a sensor and adsorbent. Its cost-effective synthesis process and compatibility with various substrates enable seamless integration into sensor platforms and adsorption systems, facilitating the development of practical solutions for real-world applications. In this respect, the performance of $C_8B_6N_6$ nanocluster as an adsorbent and sensor for the removal and detection of NA was scrutinized.

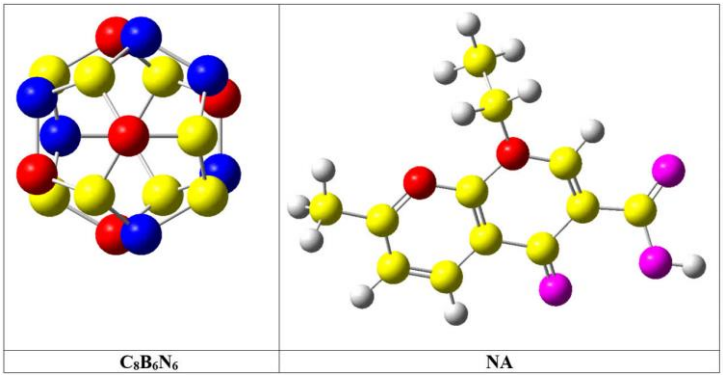

Fig. 1. The optimized structures of NA and $C_8B_6N_6$

2. Computational Details

The NA, nanocluster, and their combinations were designed using Nanotube Modeler 1.3.0.3 [27] and GaussView 6 [28] software versions, and then geometric optimization was performed for each structure. Subsequently, the optimized structures underwent various computations, including infra-red (IR), frontier molecular orbital (FMO), and natural bonding orbital (NBO) computations. The density functional theory (DFT) method, particularly the B3LYP/6-31G(*d*) level of theory, was consistently applied using Gaussian 16 [29] software version. This level of theory was chosen due to its prior acceptance and consistent alignment with experimental findings, as well as its proven reliability in predicting experimental results. This selection was made to ensure that the theoretical calculations closely correspond to the actual observations, thereby enhancing the validity and applicability of the research findings [30–35]. The study conducted computations in both gas phase and aqueous phases employing the CPCM [36] solvation method. Temperatures varying from 298 K to 318 K were examined, focusing on drug adsorption onto an adsorbent material. The goal was to comprehend how solvation and temperature impact the process, particularly in aqueous environments. This approach offers insights into the thermodynamics of drug adsorption and could potentially contribute to enhancing drug delivery systems in water-based settings [37]. The following process was scrutinized:

Drug + Adsorbent → Drug-Adsorbent (1)

We assessed the drug-adsorbent interaction by calculating adsorption energy values (E_{ad}) and various thermodynamic parameters, including the thermodynamic equilibrium constant (K_{th}), entropy changes (ΔS_{ad}), Gibbs free energy changes (ΔG_{ad}), and adsorption enthalpy changes (ΔH_{ad}) using equations 2–6 [38]. The following formulas were used for calculation of the aforementioned parameters:

$$E_{\mathrm{ad}} = \left(E_{(\mathrm{Complex})} - \left(E_{(\mathrm{Drug})} + E_{(\mathrm{Adsorbent})} + E_{(\mathrm{BSSE})}\right)\right) \quad (2)$$

$$\Delta \mathrm{H}_{\mathrm{ad}} = \left(\mathrm{H}_{(\mathrm{Complex})} - \left(\mathrm{H}_{(\mathrm{Drug})} + \mathrm{H}_{(\mathrm{Adsorbent})}\right)\right) \quad (3)$$

$$\Delta \mathrm{G}_{\mathrm{ad}} = \left(\mathrm{G}_{(\mathrm{Complex})} - \left(\mathrm{G}_{(\mathrm{Drug})} + \mathrm{G}_{(\mathrm{Adsorebnt})}\right)\right) \quad (4)$$

$$\Delta \mathrm{S}_{\mathrm{ad}} = \left(\mathrm{S}_{(\mathrm{Complex})} - \left(\mathrm{H}_{(\mathrm{Drug})} + \mathrm{H}_{(\mathrm{Adsorbent})}\right)\right) \quad (5)$$

$$\mathrm{K}_{\mathrm{th}} = \left(\exp - \left(\Delta \mathrm{G}_{\mathrm{ad}}/\mathrm{R}T\right)\right) \quad (6)$$

In the aforementioned equations, the variable *E* represents the total electronic energy for each structure being studied. E_{BSSE}, on the other hand, denotes the basis set superposition correction. The variable H encompasses the total energy of the evaluated materials along with the thermal correction of enthalpy. Similarly, G symbolizes the total energy plus the thermal correction of the Gibbs free energy, as described in reference. R refers to the constant of the ideal gas, while S represents the thermal correction entropy for the structures under investigation. Lastly, T corresponds to the temperature, as outlined in reference [39–42].

These equations, specifically equations 7–12, are utilized for the computation of several crucial properties. The bandgap (E_g), chemical hardness (η), chemical potential (μ), maximum charge capacity (ΔN_{max}), and electrophilicity (ω) of frontier molecular orbitals are all calculated using these equations [43].

$$E_{\mathrm{g}} = E_{\mathrm{LUMO}} - E_{\mathrm{HOMO}} \quad (7)$$

$$\%\Delta E_g = \frac{E_{g2} - E_{g1}}{Eg1} \times 100 \quad (8)$$

$$\eta = \left(E_{\mathrm{LUMO}} - E_{\mathrm{HOMO}}\right)/_2 \quad (9)$$

$$\mu = \left(E_{\mathrm{LUMO}} + E_{\mathrm{HOMO}}\right)/_2 \quad (10)$$

$$\omega = \mu^2/_{2\eta} \quad (11)$$

$$\Delta N_{max} = -\mu/_{\eta} \quad (12)$$

In the given equations, E_{LUMO} represents the energy of the lowest unoccupied molecular orbital, while E_{HOMO} represents the energy of the highest occupied molecular orbital. The bandgaps of the Nano-adsorbent and NM-Adsorbent complexes are denoted as Eg_1 and E_{g2}, respectively [44-48].

3. Results and Discussion

The structures of the NA-$C_8B_6N_6$ complexes are illustrated in Figure 2, showing both the initial and optimized configurations. This study focused on investigating the interaction between NA and $C_8B_6N_6$ across three different configurations in order to determine the most stable arrangement. In the A-Conformer, the nanostructure is positioned in close proximity to the ring of NA, oriented in a parallel manner. Conversely, in the B-Conformer, the adsorbent is situated near the carboxylic acid group of NA, also in a parallel orientation. Lastly, the C-Conformer places the adsorbent near the amine group of NA. Following geometrical optimization, it was clear that the adsorbate experienced a noticeable shift towards the adsorbent in all configurations, indicating a significant level of interaction between the two [35]. The computed adsorption energies, as detailed in Table 1, consistently yielded negative values, suggesting that the adsorption process is indeed feasible under experimental conditions [36]. Additionally, a thorough investigation of the influence of water as a solvent on the adsorption energies revealed that it has no significant impact on the underlying interactions [37]. This finding highlights the resilience of

the adsorption process, regardless of the presence of water as a solvent. Upon examination, it is clear that the presence of water has little effect on the modification of adsorption energies. Following geometric optimizations, the analyzed structure underwent IR computations, leading to the determination of minimum and maximum frequencies as specified in Table 1. All computed frequencies resulted in positive values, indicating that all structures under scrutiny represent true local minima. This result confirms the stability of the examined structures [38]. Moreover, the table in Table 1 presents dipole moment values, showcasing significant alterations in the dipole moment values following the adsorption of NA onto the surface of $C_8B_6N_6$. This finding suggests a notable improvement in the solubility and chemical reactivity of NA when it is adsorbed on the nanocluster [39]. Amongst the configurations investigated, C-Conformer exhibited the most negative adsorption energy value, indicating that the formation of this configuration is more favorable than others.

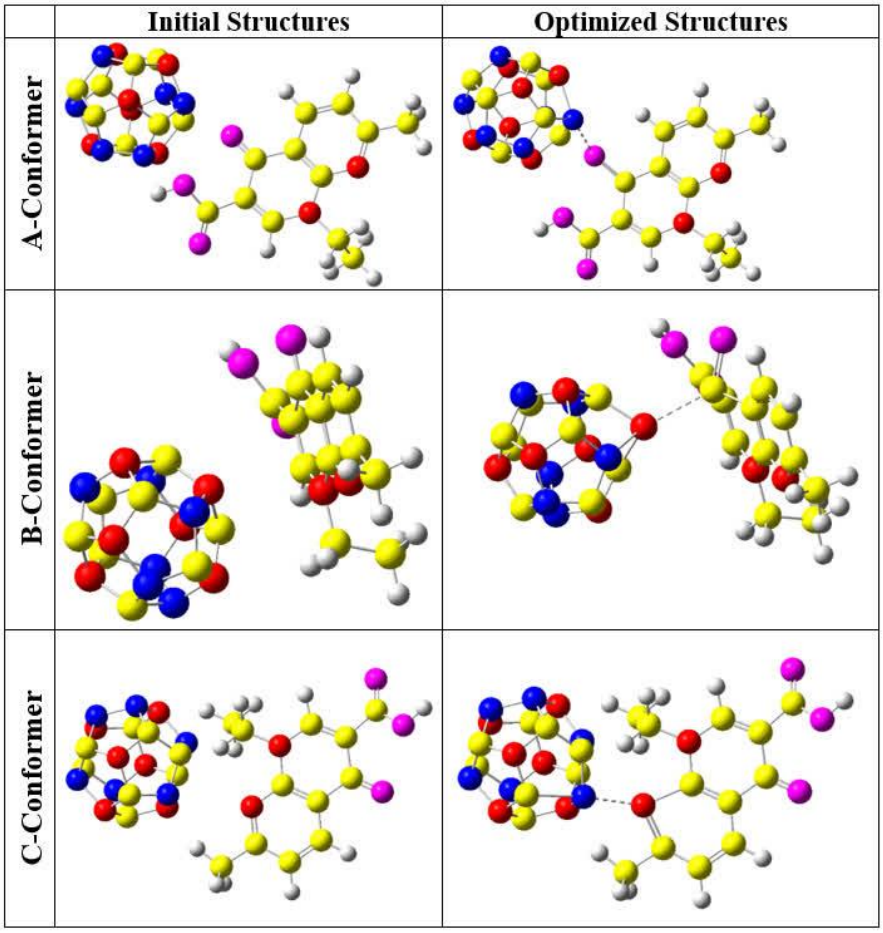

Fig. 2. The initial and optimized structures

Table 1. Structural properties

NO	Adsorption energy (kJ/mol)	Zero-point energy (kJ/mol)	ν_{min} (cm^{-1})	ν_{max} (cm^{-1})	Dipole moment (Deby)
NA (Gas phase)	---	699.67	41.77	4219.09	2.13
NA (Water)	---	701.97	42.01	4317.28	2.87
$C_8B_6N_6$ (Gas phase)	---	283.50	372.64	1641.03	0
$C_8B_6N_6$ (Water)	---	292.96	374.02	1637.39	0.02
A-Conformer (Gas phase)	-81.15	1096.11	17.97	3768.01	5.89
A-Conformer (Water)	-66.89	1100.81	19.69	3768.65	6.23
B-Conformer (Gas phase)	-45.39	1112.78	11.11	4221.89	7.67
B-Conformer (Water)	-33.88	1097.46	11.95	4224.13	8.68
C-Conformer (Gas phase)	-107.55	1101.96	11.34	4307.05	9.33
C-Conformer (Water)	-88.66	1106.27	13.80	4309.12	9.99

The thermodynamic parameters reported in Table 2 demonstrate an exothermic and spontaneous interaction between NA and $C_8B_6N_6$, as evidenced by the negative values of ΔH_{ad} and ΔG_{ad} [40]. Furthermore, the study investigated the impact of temperature and solvent on these interactions and found that neither factor significantly influenced the thermodynamic parameters [41]. Interestingly, the negative values of ΔSad suggest that the adsorption process is unfavourable in terms of entropy, indicating the aggregation of nanostructures after the drug adsorption [42].

Table 2. The calculated Thermodynamic parameters

Structure-phase-Temperature (K)	ΔH_{ad} (kJ/mol)	ΔG_{ad} (kJ/mol)	ΔS_{ad} (J/mol)
A-Conformer-gas-298	-101.81	-45.69	-184.44
A-Conformer-gas-308	-100.01	-39.82	-62.33
A-Conformer-gas-318	-98.22	-33.95	-189.56
A-Conformer-Water-298	-8.83	-45.70	-178.65
A-Conformer-Water-308	-7.03	-38.57	-181.22
A-Conformer-Water-318	-5.23	-31.46	-184.77
B-Conformer-gas-298	-69.62	-18.90	-166.25
B-Conformer-gas-308	-67.81	-14.92	-168.81
B-Conformer-gas-318	-66.01	-10.93	-171.38
B-Conformer-Water-298	-58.11	-7.40	-176.76
B-Conformer-Water-308	-56.32	-5.49	-174.62
B-Conformer-Water-318	-54.51	-3.59	-177.19
C-Conformer-gas-298	-127.21	-71.10	-179.29
C-Conformer-gas-308	-125.41	-67.89	-181.85
C-Conformer-gas-318	-123.61	-64.68	-184.42
C-Conformer-Water-298	-117.32	-71.10	-172.44
C-Conformer-Water-308	-115.53	-65.69	-175.01
C-Conformer-Water-318	-113.72	-60.28	-177.57

The data presented in Table 3 provides clear evidence of the significant impact of NA adsorption on the properties of $C_8B_6N_6$. It is evident that the bandgap of $C_8B_6N_6$ undergoes a notable shift from 8.09 eV to 5.46, 6.07, and 6.32 eV for A, B, and C conformers, respectively, indicating a substantial alteration in bandgap during the adsorption process. This observation suggests that the evaluated nanocluster has the potential to serve as an effective modifier for electrocatalytic detection of NA. Furthermore, it is noteworthy that the chemical hardness of NA experiences a considerable decrease upon interaction with $C_8B_6N_6$, implying an enhanced chemical reactivity. The increasing of chemical potential also confirms it. Additionally, when NA interacts with the $C_8B_6N_6$ surface, it leads to a noticeable decrease in both electrophilicity and maximum transferred charge capacity, implying a lower tendency for electron absorption. In summary, these results strongly indicate that NA-$C_8B_6N_6$ complexes demonstrate elevated chemical reactivity compared to pure NA without a nanostructure present.

Table 3. The calculated FMO parameters

NO	**E_{HOMO} (eV)**	**E_{LUMO} (eV)**	**Eg (eV)**	**%ΔEg**	**η (eV)**	**μ (eV)**	**ω (eV)**	**ΔNmax (eV)**
NA	-5.61	4.87	10.48	---	5.24	-0.37	0.01	0.07
$C_8B_6N_6$	-5.62	2.47	8.09	---	4.05	-1.58	0.31	0.39
A-Conformer	-2.45	3.01	5.46	-32.46	2.73	0.28	0.01	-0.10
B-Conformer	-2.87	3.20	6.07	-24.97	3.04	0.17	0.00	-0.05
C-Conformer	-3.01	3.31	6.32	-21.88	3.16	0.15	0.00	-0.05

5. Conclusion

The research conducted an examination of the effectiveness of $C_8B_6N_6$ nanocluster in serving as both an adsorbent and sensor for the removal and detection of NA through the use of density functional theory computations. The results of the study demonstrated that there is a feasible, exothermic, and spontaneous interaction between NA and $C_8B_6N_6$, thereby indicating the potential of $C_8B_6N_6$ as an efficient adsorbent for the removal of NA. Furthermore, the research delved into investigating the influence of water as the solvent and varying temperature on the thermodynamic parameters, ultimately revealing that these factors did not significantly impact the interactions. In addition, the Frontier Molecular Orbital (FMO) analysis unveiled noteworthy changes in the bandgap of $C_8B_6N_6$ from 8.09 (eV) to 5.46 (eV) (-32.46%) during the adsorption process, thus suggesting its potential utility as an effective electrocatalytic modifier for the electrochemical detection of NA. The study also discussed other FMO parameters in detail. In conclusion, this study provides valuable insights into the potential use of $C_8B_6N_6$ as an efficient adsorbent and sensor for the removal and detection of NA.

References

[1] I. Robinson, G. Junqua, R. Van Coillie and O. Thomas, Trends in the detection of pharmaceutical products, and their impact and mitigation in water and wastewater in North America. Anal. Bioanal. Chem., 387 (2007) 1143–1151.

[2] A. Ghauch, A. Tuqan and H. A. Assi, Antibiotic removal from water: Elimination of amoxicillin and ampicillin by microscale and nanoscale iron particles. Environ. Pollut., 157 (2009) 1626–1635.

[3] A. L. Spongberg and J. D. Witter, Pharmaceutical compounds in the wastewater process stream in Northwest Ohio. Sci. Total Environ., 397 (2008) 148–157.

[4] E. Yabalak, Degradation of ticarcillin by subcritical water oxidation method: application of response surface methodology and artificial neural network modeling. J. Environ. Sci. Heal. A, 53 (2018) 975–985.

[5] M. Ahmadi, T. Madrakian and A. Afkhami, Solid phase extraction of amoxicillin using dibenzo-18-crown-6 modified magnetic-multiwalled carbon nanotubes priortoits spectrophotometric determination. Talanta, 148 (2016) 122–128.

[6] F. J. Benitez, J. L. Acero, F. J. Real, G. Roldan and F. Casas, (2011). Comparison of differentchemical oxidation treatments for the removal of selected pharmaceuticals in water matrices. Chem. Eng. J., 168 (2011) 1149–1156.

[7] S. M. Mitchell, J. L. Ullman, A. L. Teel and R.J. Watts, Hydrolysis of amphenicol and marcrolide antibiotics: Chloramphenicol, florfenicol, spiramycin, and tylosin. Chemosphere.,134 (2015) 504–511.

[8] Y. Ji, Y. Shi, W. Dong, X. Wen, M. Jiang and J. Lu, Thermo-activated persulfate oxidation system for tetracycline antibiotics degradation in aqueous solution. Chem. Eng. J., 298 (2016) 225–233.

[9] R. S. Bangari and N. Sinha, Adsorption of tetracycline, ofloxacin and cephalexin antibiotics on boron nitride nanosheets from aqueous solution. J. Mol. Liq., 293 (2019) 1–12.

[10] B. H. Hameed, A. M. Din and A. L. Ahmad, Adsorption of methylene blue onto bamboo-based activated carbon: kinetics and equilibrium studies, J. Hazard. Mater., 141 (2007) 819–825.

[11] E. Alvarez-Ayuso, A. Garcıa-Sánchez and X. Querol, Purification of metal electroplating wastewaters using zeolites. Water Res., 37 (2003) 4855–4862.

[12] Y. Yao, B. He, F. F. Xu and X. F. Chen, Equilibrium and kinetic studies of methylorange adsorption on multiwalled carbon nanotubes. Chem. Eng. J., 170 (2011) 82–89.

[13] S. Zeng, K. Tang, T. Li and Z. Liang. 3D flower-like Y2O3: Eu3+ nanostructures: template-free synthesis and its luminescence properties. J. Colloid Interface Sci., 316 (2007) 921–929.

[14] A. K. Rahardjo, M. J. J. Susanto, A. Kurniawan, N. Indraswati and S. Ismadji, Modified Ponorogo bentonite for the removal of ampicillin from wastewater. J. Hazard. Mater., 190 (2011) 1001–1008.

[15] P. Del Vecchio, N. K. Haro, F.S. Souza, N. R. Marcílio and L. A. Féris, Ampicillin removal by adsorption onto activated carbon: kinetics, equilibrium and thermodynamics. Water Sci Technol., 79 (2019) 2013–2021.

[16] F. S. Souza and L. A. Féris, Consumption-based approach for pharmaceutical compounds in a large hospital. Environ. Technol., 38 (2017) 2217–2223.

[17] X. Weng, W. Cai, R. Lan, Q. Sun and Z. Chen, Simultaneous removal of amoxicillin, ampicillin and penicillin by clay supported Fe/Ni bimetallic nanoparticles. Environ. Pollut., 236 (2018) 562–569.

[18] V. Nairi, L. Medda, M. Monduzzi and A. Salis, Adsorption and release of ampicillin antibiotic from ordered mesoporous silica. J. Colloid Interface Sci., 497 (2017) 217–7225.

[19] S. Yu, X. Wang, H. Pang, R. Zhang, W. Song, D. Fu, T. Hayat and X. Wang, Boron nitride-based materials for the removal of pollutants from aqueous solutions: A review. Chem. Eng. J., 333 (2018) 343–360.

[20] S. N. Naess, A. Elgsaeter, G. Helgesen and K. D. Knudsen, (2009) Carbon nanocones: wall structure and morphology. Sci. Tchnol. Adv. Mater., 10 (2009) 065002.

[21] (a) S. Esfahani, J. Akbari, S. Soleimani-Amiri, M. Mirzaei, and A. Ghasemi Gol. Assessing the drug delivery of ibuprofen by the assistance of metal-doped graphenes: insights from density functional theory. *Diamond and Related Materials* 135 (2023) 109893. (b) K. Silas, Y. P. Musa, M. D. Habiba, Effective Application of Jatropha Curcas Husk Activated ZnCl2 for Adsorption of Methylene Blue: Isotherm, Kinetics and Development of Empirical Model, Chem. Rev. Lett. 6 (2022) 153-160. (c) A. Hosseinian, S. Soleimani-Amiri, S. Arshadi, E. Vessally,

and L. Edjlali. Boosting the adsorption performance of BN nanosheet as an anode of Na-ion batteries: DFT studies. *Physics Letters A* 381(24) (2017) 2010-2015. (d) A. Yadav, A. Taha, Y. A. Abdulsayed, S. M. Saeed, A Density Functional Theory (DFT) Study on Adsorption of a biological active ethionamide over the Surface of a Fe-decorated porphyrin system, Chem. Rev. Lett. 6 (2023) 128-138. (e) A. Ahmadpour, Using of Activated Carbon Adsorption in Wastewater Industries, J. Chem. Lett. 3 (2022) 2-9.

[22] (a) G. N. Zaharaddeen, S. Godwill, P. A. Ekwumemgbo, Split Plot Central Composite Design for Optimization of 4-Bromophenol Adsorption from Synthetic Wastewater, using Synthesized BiFeO3 Perovskite Material, Chem. Rev. Lett. 6 (2023) 150-165. (b) E. Vessally, S. Soleimani-Amiri, A. Hosseinian, L. Edjlali, A. Bekhradnia,The Hartree-Fock exchange effect on the CO adsorption by the boron nitride nanocage, Physica E Low Dimens. Syst. Nanostruct., 87 (2017) 308–311. (c) N. S. Yapo, K. E. Adou, J. Ano, D. N. Nonh, K. B. Yao, Adsorption of fluoride ions on hydroxyapatite-modified Corbula trigona shell waste: Effect of coexisting anions, temperature and regeneration, J. Chem. Lett. 4 (2023) 95-102. (d) A. S. Hessen, N. M. A. Alsultany, H. Bahir, A. H. Adthab, S. Soleimani-Amiri, S. Ahmadi, E. Vessally, A. Khanmohammadi, Adsorption of sulfur mustard on the transition metals (TM = Ti2+,Fe2+,Co2+, Ni2+, Cu2+, Zn2+) porphyrins induced in carbon nanocone (TM-PCNC): Insight from DFT calculation, J. Mol. Graph. 135 (2025) 108928. (e) R. Kaviani, Investigation of the Application of Zeolites in the Adsorption Mechanism, J. Chem. Lett. 3 (2022) 10-19.

[23] M. Mirzaei, M. Yousefi and M. Meskinfam, Chemical shielding properties for BN, BP, AI N, and AIP nanocones: DFT studies, Superlattices Microst., 51 (2012) 809–813.

[24] Y. Li, Y. Tian, Ch. Yang, K. Cai and D. Zhang, Torsional properties of boron nitride nanocones with different cone heights, disclination angles and simulation temperatures Nano, 10 (2015) 1550097.

[25] G. Lian, X. Zhang, S. Zhang, D. Liu, D. Cui and Q. Wang, Controlled fabrication of ultrathin-shell BN hollow spheres with excellent performance in hydrogen storage and wastewater treatment. Energy Environ. Sci., 5 (2012) 7072-7080.

[264] X. Zhang, G. Lian, S. Zhang, D. Cui and Q. Wang, Boron nitride nanocarpets: controllable synthesis and their adsorption performance to organic pollutants. Cryst. Eng. Comm., 14 (2012) 4670–4676.

[27] Nanotube Modeler J. Crystal. Soft., 2014 software.

[28] GaussView, Version 6.1, R. Dennington, T. A. Keith, J. M. Millam, Semichem Inc., Shawnee Mission, KS, 2016.

[29] Gaussian 16, Revision C.01, M. J. Frisch, G. W. Trucks, H. B. Schlegel, G. E. Scuseria, M. A. Robb, J. R. Cheeseman, G. Scalmani, V. Barone, G. A. Petersson, H. Nakatsuji, X. Li, M. Caricato, A. V. Marenich, J. Bloino, B. G. Janesko, R. Gomperts, B. Mennucci, H. P. Hratchian, J. V. Ortiz, A. F. Izmaylov, J. L. Sonnenberg, D. Williams-Young, F. Ding, F. Lipparini, F. Egidi, J. Goings, B. Peng, A. Petrone, T. Henderson, D. Ranasinghe, V. G. Zakrzewski, J. Gao, N. Rega, G. Zheng, W. Liang, M. Hada, M. Ehara, K. Toyota, R. Fukuda, J. Hasegawa, M. Ishida, T. Nakajima, Y. Honda, O. Kitao, H. Nakai, T. Vreven, K. Throssell, J. A. Montgomery, Jr., J. E. Peralta, F. Ogliaro, M. J. Bearpark, J. J. Heyd, E. N. Brothers, K. N. Kudin, V. N. Staroverov, T. A. Keith, R. Kobayashi, J. Normand, K. Raghavachari, A. P. Rendell, J. C. Burant, S. S. Iyengar, J. Tomasi, M. Cossi, J. M. Millam, M. Klene, C. Adamo, R. Cammi, J. W. Ochterski, R. L. Martin, K. Morokuma, O. Farkas, J. B. Foresman, and D. J. Fox, Gaussian, Inc., Wallingford CT, 2016.

[30] N. M. O'Boyle, A. L. Tenderholt, K. M. Langner, A Library for Package-Independent Computational Chemistry Algorithms. J. Comp. Chem., 29 (2008) 839-845.

[31] R. Ahmadi, M. R. Jalali Sarvestani, Adsorption of Tetranitrocarbazole on the Surface of Six Carbon-Based Nanostructures: A Density Functional Theory Investigation. Phys. Chem. B., 14 (2020) 198-208.

[32] M. R. Jalali Sarvestani, R. Ahmadi, Adsorption of TNT on the surface of pristine and N-doped carbon nanocone: A theoretical study. Asian J. Nanosci. Mater., 3 (2020) 103-114.

[33] M. R. Jalali Sarvestani, M. Gholizadeh Arashti, B. Mohasseb, Quetiapine Adsorption on the Surface of Boron Nitride Nanocage (B12N12): A Computational Study. Int. J. New. Chem., 7 (2020) 87-100.

[34] M. R. Jalali Sarvestani, R. Ahmadi, Investigating the Complexation of a recently synthesized phenothiazine with Different Metals by Density Functional Theory. Int. J. New. Chem., 4 (2017) 101-110.

[35] M. R. Jalali Sarvestani, R. Ahmadi, Adsorption of Tetryl on the Surface of B12N12: A Comprehensive DFT Study. Chem. Methodol., 4 (2020) 40-54.

[36] S. Majedi, F. Behmagham, M. Vakili, Theoretical view on interaction between boron nitride nanostructures and some drugs. J. Chem. Lett., 1 (2020) 19-24.

[37] H. G. Rauf, S. Majedi, E. A. Mahmood, M. Sofi, Adsorption behavior of the Al- and Ga-doped B12N12 nanocages on COn (n=1, 2) and HnX (n=2, 3 and X=O, N): A comparative study. Chem. Rev. Lett., 2 (2019) 140-150.

[38] R. A. Mohamed, U. Adamu, U. Sani, S. A. Gideon, A. Yakub, Thermodynamics and kinetics of 1-fluoro-2-methoxypropane vs Bromine monoxide radical (BrO): A computational view. Chem. Rev. Lett., 2 (2019) 107-117.

[39] S. Majedi, H. G. Rauf, M. Boustanbakhsh, DFT study on sensing possibility of the pristine and Al- and Ga-embeded B12N12 nanostructures toward hydrazine and hydrogen peroxide and their analogues. Chem. Rev. Lett. 2 (2019) 176-186.

[40] R. Moladoust, Sensing performance of boron nitride nanosheets to a toxic gas cyanogen chloride: Computational exploring. Chem. Rev. Lett., 2 (2019) 151-156.

[41] M. R. Jalali Sarvestani, Z. Doroudi, Fullerene (C20) as a potential sensor for thermal and electrochemical detection of amitriptyline: A DFT study. J. Chem. Lett., 1 (2020) 63-68.

[42] S. Majedi, F. Behmagham, M. Vakili, Theoretical view on interaction between boron nitride nanostructures and some drugs. J. Chem. Lett. 1 (2020) 19-24.

[43] S. A. Siadati, M. A. Ebrahimzadeh, Rezvan Yazdian-Robati, and E. Babanezhad. A theoretical approach on the possibility of using α-phographene, g-X3N4 nanosheets, and C19X fullerenes for adsorption and drug delivery of a proteasome inhibitor drug. *Diamond and Related Materials* 147 (2024) 111344.

[44] S. Soleimani-Amiri, M. Koohi, B. Mirza. Characterizations of B and N heteroatoms as substitutional doping on structure, stability, and aromaticity of novel heterofullerenes evolved from the smallest fullerene cage C_{20}: a density functional theory perspective. J. Phys. Org. Chem., 29(10) (2016) 514-522.

[45] M. Koohi, S. Soleimani-Amiri, M. Shariati. Silicon impacts on structure, stability and aromaticity of C20-nSin heterofullerenes (n= 1–10): A density functional perspective. J. Mol. Struct., 1127 (2017) 522-531.

[46] M. Koohi, S. Soleimani Amiri, and B. N. Haerizade. Substituent effect on structure, stability, and aromaticity of novel BnNmC20–(n+ m) heterofullerenes. J. Phys. Org. Chem., 30 (2017) e3682.

[47] M. Koohi, M. Shariati, and S. Soleimani Amiri. A comparative study on the Ge6C14 heterofullerene nanocages: a density functional survey. J. Phys. Org. Chem., 30 (2017) e3678.

[48] M. Koohi, S. Soleimani-Amiri, M. Shariati. Novel X-and Y-substituted heterofullerenes X4Y4C12 developed from the nanocage C 20, where X= B, Al, Ga, Si and Y= N, P, As, Ge: a comparative investigation on their structural, stability, and electronic properties at DFT. Struct. Chem. 29 (2018) 909-920.